Metal-Insulator Transition in the Amorphous CexSi100-x (4 x 83) Heavy Fermion System

Materials Transactions, Vol. 42, No. 6 (2001) pp. 939 to 950
Special Issue on Struture and Electronic Properties in the Pseudogap Systems

OVERVIEW

Metal-Insulator Transition in the Amorphous Ce_xSi_{100-x} ($4 \leq x \leq 83$) Heavy Fermion System

Tetsushi Biwa, Masaaki Yui *, Tsunehiro Takeuchi and Uichiro Mizutani

Department of Crystalline Materials Science, Nagoya University, Nagoya 464-8603, Japan

The electronic structure, magnetic properties and electron transport properties have been studied on amorphous Ce_xSi_{100-x} ($4 \leq x \leq 83$) alloys in comparison with non-magnetic amorphous La_xSi_{100-x} ($11 \leq x \leq 63$) and Ti_xSi_{100-x} ($6 \leq x \leq 41$) alloys with a particular emphasis on the formation of the pseudogap at the Fermi level and its effect on the electron transport upon approaching the metal-insulator transition in the heavy fermion system. It is shown that the interaction between conduction electrons and localized moments leads to an anomalous enhancement in the temperature dependence of the measured resistivity below 10 K. We also revealed that the amorphous Ce_xSi_{100-x} alloy system crosses the metal-insulator transition at about 12 at%Ce and that the marginally metallic $Ce_{15}Si_{85}$ alloy has the resistivity of 1500 μΩcm comparable to those in the non-magnetic reference systems but a large electronic specific heat coefficient γ of 22 mJ/mol·K^2, which is 50 times as large as the value of 0.4 mJ/mol·K^2 for the marginally metallic $Ti_{13}Si_{87}$ alloy. The set of ($\rho_{300\,K}$, γ_{exp}) data fall on an extremely small diffusion constant line in the ρ-γ diagram. This unique behavior is attributed to the existence of Ce-4f electrons at the Fermi level, which give rise to a large value of γ but are localized and immobile even in the metallic regime.

(Received January 12, 2001; Accepted May 1, 2001)

Keywords: *metal-insulator transition, heavy fermion, specific heat, localization, pseudogap system, incoherent Kondo effect*

1. Introduction

The pseudogap is formed across the Fermi level E_F through different mechanisms. The concept of the pseudogap was originally introduced by Mott[1] in relation to the metal-insulator transition in expanded liquid mercury. Indeed, the formation of the pseudogap was experimentally confirmed through measurements of the Hall coefficient and electrical resistivity upon an expansion of volume at high temperatures under high pressures in liquid mercury.[2] In quasicrystals and their approximants, simultaneous contacts of the Fermi surface with many Brillouin zone planes are responsible for its formation.[3–5] In amorphous M_xX_{100-x} alloy systems, where M and X stand for a metal and metalloid element, respectively, the metal-insulator transition occurs when the concentration x of a metallic element M is decreased below some critical value. Obviously, a finite energy gap exists at $x = 0$ corresponding to the pure element X like amorphous Si or Ge. Hence, the transition from a metal to an insulator with decreasing the metal content does occur in amorphous M_xX_{100-x} alloy systems, which can be viewed as the process of deepening the pseudogap across E_F.

Electron transport properties were systematically studied together with both atomic and electronic structures across the metal-insulator transition in amorphous V_xSi_{100-x} ($7 \leq x \leq 74$)[6] and Ti_xSi_{100-x} ($6 \leq x \leq 41$) alloys.[7] Tanaka *et al.* have also studied the electronic structure near the Fermi level in amorphous Pd_xSi_{100-x} alloys over the composition range covering the metal-insulator transition by means of the photoemission spectroscopy measurements.[8] In the case of amorphous V_xSi_{100-x} alloy system, a decrease in the V concentration lowers the V-3d density of states at E_F and eventually leads to a semiconducting amorphous Si. Thus, this is typical of the pseudogap system. The conductivity for alloys with $x > 20$ can be well explained in terms of the quantum interference effect characteristic of a disordered metallic system whereas those with $x < 15$ in terms of the variable-range hopping model applicable to an insulating regime. Therefore, the metal-insulator transition in the amorphous V_xSi_{100-x} alloys occurs in the composition range 15–20 at%V. Similarly, the metal-insulator transition is claimed to occur at about 9.5 at%Ti in the amorphous Ti_xSi_{100-x} alloys.

Mizutani plotted the room temperature resistivity against the measured electronic specific heat coefficient for a large number of amorphous alloys and quasicrystals to extract universal features of the metal-insulator transition in many different systems.[3] Here the measured electronic specific heat coefficient is assumed to represent the density of states (DOS) at E_F, $N(E_F)$. It was further assumed that, in metallic side of the metal-insulator transition, all electrons including both sp- and d-electrons at E_F contribute equally to the electron conduction and that the conductivity formula $\sigma = \frac{e^2}{3}\Lambda_F v_F N(E_F)$ is applicable to them, where Λ_F is the mean free path of conduction electrons and v_F is the Fermi velocity. Furthermore, conduction electrons near the metal-insulator transition are assumed to take a minimum diffusion coefficient $D_{min}\left(= \frac{\Lambda_F^{min} v_F^{min}}{3}\right)$ equal to 0.25 cm^2/s, which is simply deduced by using Λ_F^{min} equal to an average atomic distance of 0.3 nm and v_F^{min} equal to one-fourth of the free electron Fermi velocity, namely, 0.25×10^8 cm/s. Its justification has been discussed elsewhere.[3] A line $\rho = (\pi^2/3)(k_B/e)^2 D_{min}^{-1}\gamma^{-1}$ with a slope of -1 can be drawn in the ρ-γ diagram on the log-log scale. This is called the metal-insulator transition line (MI-line). Indeed, almost all data for non-magnetic amorphous alloys and quasicrystals in metallic regime were found to fall below the MI-line.[3]

An unusually large electronic specific heat coefficient γ has been reported in intermetallic compounds based on rare earth elements Ce and Yb.[9,10] They are known as heavy fermion systems. The 4f-electrons are believed to be not only responsible for the formation of the localized magnetic moment but

*Graduate Student, Nagoya University.

also for the possession of an extremely large value of γ. A large enhancement in γ has been observed also in amorphous Ce_xSi_{100-x} alloys in the metallic regime.[11] It is therefore of great challenge to examine how amorphous Ce_xSi_{100-x} alloys enter the metal-insulator transition with decreasing Ce content on the ρ-γ diagram and to discuss the electron transport mechanisms by making full use of the ρ-γ diagram thus obtained. The amorphous La_xSi_{100-x} alloys were also synthesized in this experiment to use the data as a reference together with those for amorphous Ti_xSi_{100-x} and V_xSi_{100-x} alloys reported earlier, since they are free from 4f-electrons.

2. Experimental Details

An alloy ingot was prepared in button form, 30 mm in diameter and about 10 mm in thickness by arc melting of appropriate amounts of pure Si (99.999%), pure Ce (99.9%) and pure La (99.9%). The composition of the ingot was checked by means of EPMA (electron probe micro-analysis) method. Even after repeated arc-melting and turning of the ingot, a small difference in composition was observed between the top and bottom surfaces in some Ce_xSi_{100-x} samples. In particular, the ingots in the vicinity of 30 at%Ce could not be homogeneously alloyed and the composition difference exceeded 2 at% between the top and bottom surfaces. Thus, amorphous samples in the composition range $25 < x < 35$ were abandoned.

The homogeneously mixed ingot was used as a target for the triode DC sputtering. The backpressure in the vacuum chamber was evacuated to 4×10^{-5} Pa before the introduction of pure Ar gas. During the deposition, the Ar gas pressure was maintained at 5.3×10^{-3} Pa. The distance between the target and substrate was 25 mm. The sputtering rate was about several nm·min^{-1}. The film was deposited onto Cu plate up to about several 10 μm in thickness and was mechanically peeled off from the substrate.

The X-ray diffraction spectra were taken with Cu-Kα radiation. The formation of an amorphous single phase was confirmed by the appearance of a halo pattern without any Bragg peaks. The composition of the film was studied by the EPMA and ion-coupled plasma (ICP) methods. The deviation from the nominal composition was found to be within ±1 at%. An amorphous single phase was obtained in the composition ranges $4 \leq x \leq 83$ and $11 \leq x \leq 63$ in the Ce_xSi_{100-x} and La_xSi_{100-x} systems, respectively. The thermal stability of an amorphous phase was studied by using a differential scanning calorimeter (DSC) (RIGAKU-8131BH). Each sample weighing about 10–20 mg, was sealed in a Ag pan and heated in Ar-gas flowing atmosphere with a heating speed of 15 K min^{-1} in the temperature range up to 1073 K.

The electrical resistivity was measured by using a four-probe DC method over the temperature range 1.8–300 K in magnetic fields of 0–9 T (Quantum Design Inc., PPMS-9L). The magnetic susceptibility was also measured over the temperature range 1.8–300 K in magnetic fields 0–7 T (Quantum Design Inc., MPMS7). The low temperature specific heat was studied by using the relaxation technique in the temperature range 0.5–30 K in magnetic fields of 0–5 T (Oxford Instruments, MLHC9H). The X-ray photoemission spectroscopy measurement was carried out at room temperature for a series of amorphous Ce_xSi_{100-x} alloys by using the monochromated Al-Kα radiation (SSI Inc., SSX-100). In addition, high-resolution ultra-violet photoemission spectrum was measured at 8 K for the amorphous $Ce_{15}Si_{85}$ alloy together with pure Au as a reference, using a Scienta SES2002 hemispherical analyzer with a Gammadata VUV5010 photon source ($h\nu$ = 21.218 eV) at the Institute of Solid State Physics, the University of Tokyo. The Seebeck coefficient was measured with a commercially available apparatus (MMR Technologies, SB-100) in the temperature range 100–400 K.

3. Experimental Results

3.1 Thermal stability of amorphous phase

Figure 1 shows the Ce concentration dependence of the crystallization temperature T_x for amorphous Ce_xSi_{100-x} alloys. A single-step crystallization into Si crystallites was observed in the Ce concentration range up to 10 at%. When the Ce concentration exceeds 13 at%, a two-step crystallization was observed: the higher one into the Si crystallites and the lower one into the $CeSi_2$-type precipitates. The crystallization temperature could not be determined for samples containing more than 30 at%Ce because of rapid oxidation upon heating in the DSC cell.

3.2 Electrical resistivity measurements

The room temperature conductivity is plotted on the logarithmic scale against the solute concentration in Fig. 2 for a series of amorphous Ce_xSi_{100-x} and La_xSi_{100-x} alloys together with the data for amorphous Ti_xSi_{100-x} alloys.[7] Nu-

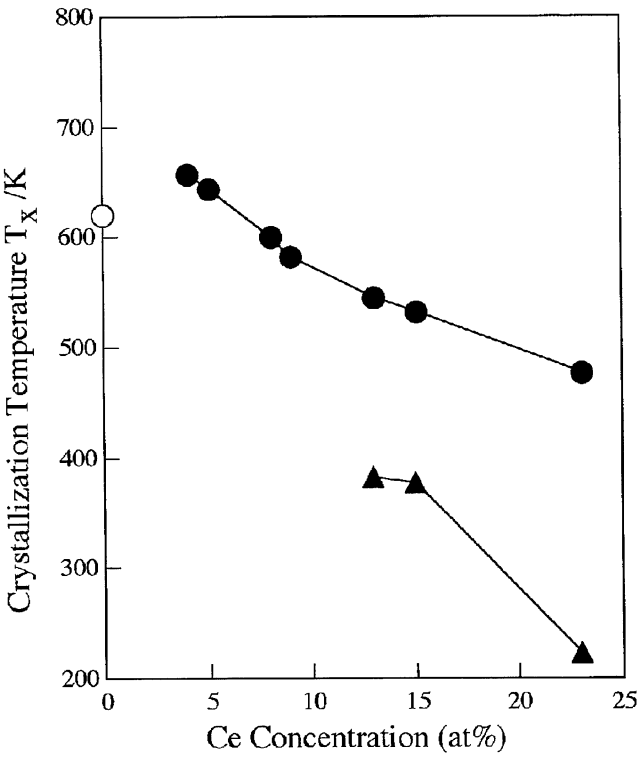

Fig. 1 Ce concentration dependence of crystallization temperature in amorphous Ce_xSi_{100-x} alloys. Symbols (●) and (▲) indicate the crystallization into Si- and $CeSi_2$-type precipitates, respectively. Symbol (○) refers to the crystallization temperature of amorphous Si in literature.

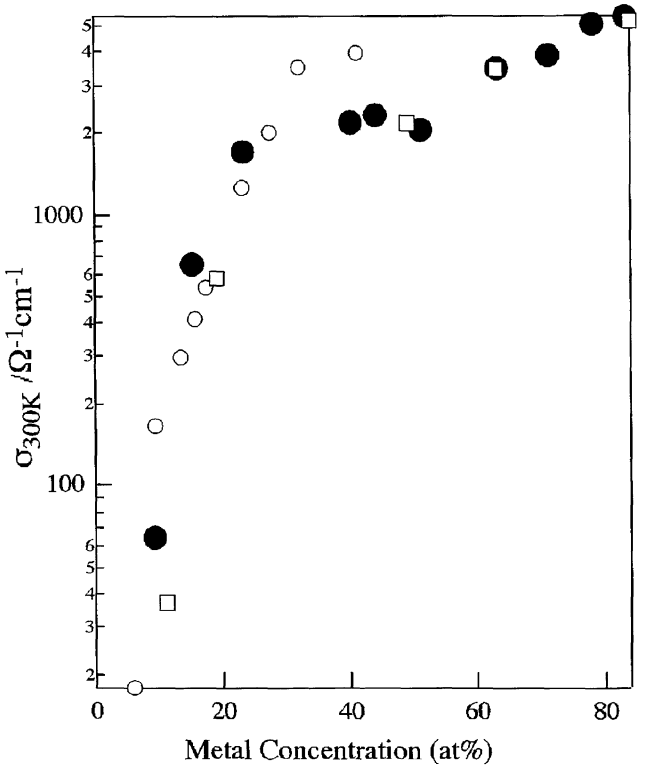

Fig. 2 Metal concentration dependence of conductivity at 300 K in amorphous Ce_xSi_{100-x} (●) and La_xSi_{100-x} (□) alloys measured in this experment together with the data for the amorphous Ti_xSi_{100-x} (○) alloys.[7]

Table 1 Electronic Properties of amorphous Ce_xSi_{100-x} alloys.

x (at%Ce)	$\rho_{300\,K}$ (μΩ-cm)	γ mJ/mol·K^2	$S_{300\,K}$ (μV/K)
4	2610000	0.14	—
9	15420	12.0	−55
15	1523	22.5	—
23	—	—	−25
40	—	—	− 8
51	478	87.6	—
63	289	113.8	− 8
83	—	—	− 3

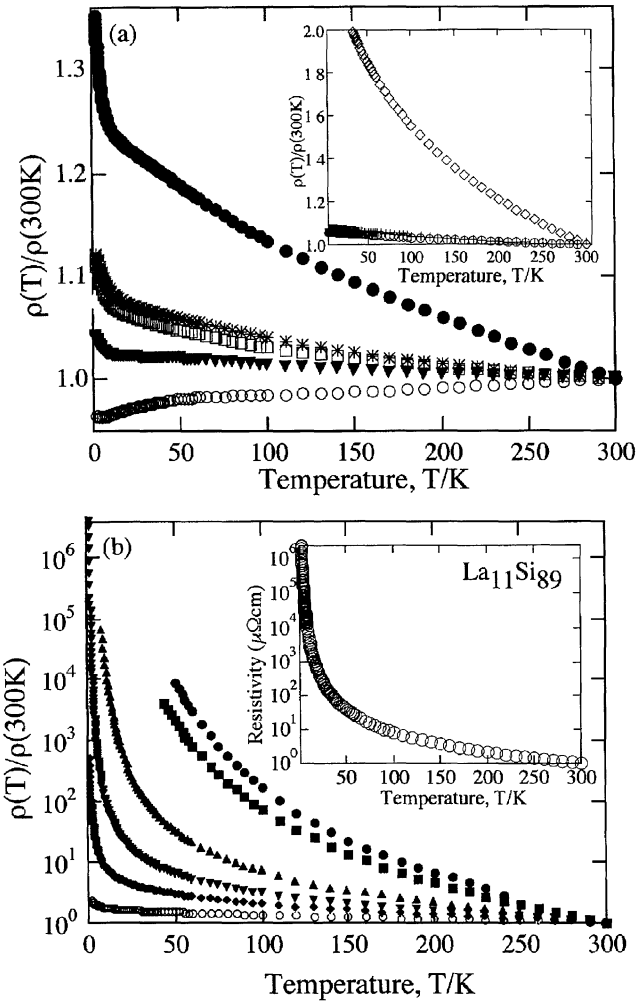

Fig. 3 Temperature dependence of the electrical resistivity for amorphous Ce_xSi_{100-x} alloys with different compositions (a) (●) $x = 23$, (□) $x = 40$, (✻) $x = 51$, (▼) $x = 71$, (●) $x = 83$ and (b) (●) $x = 4$, (■) $x = 6$, (▲) $x = 8$, (▼) $x = 9$, (◆) $x = 12$ and (○) $x = 15$. Insets show the data for amorphous La_xSi_{100-x} alloys with different compositions: (◇) $x = 19$, (+) $x = 49$, (○) $x = 63$ in (a) and $La_{11}Si_{89}$ in (b). The resistivity value is normalized with respect to that at 300 K except for the data in inset (b).

merical data on the room temperature resistivity is listed in Table 1 together with the electronic specific heat coefficient and Seebeck coefficient described below. It is clear that the value of conductivity decreases with decreasing the concentration of the solute M (= Ce, La and Ti) and falls below 100 Ω^{-1}cm^{-1} in the range below about 10 at%, regardless of whether 4f electrons are involved or not. If we accept the empirical rule that the metal-insulator transition is encountered when the conductivity is decreased below 100–200 Ω^{-1}cm^{-1}, then the metal-insulator transition most likely occurs in the Ce concentration range around 10 at% in amorphous Ce_xSi_{100-x} alloy system.

The temperature dependences of electrical resistivity for amorphous Ce_xSi_{100-x} alloys with $x \geq 23$ and $x \leq 15$ are plotted in Figs. 3(a) and (b) over the temperature range 1.8–300 K, respectively. For comparison, the data for the non-magnetic amorphous La_xSi_{100-x} alloys are shown in the insets. The temperature coefficient of resistivity defined as $(1/\rho)$ $(d\rho/dT)$ is negative for all samples except for the 83 at%Ce alloy. A sharp increase in slope is observed below about 10 K for amorphous Ce_xSi_{100-x} alloys with solute concentrations higher than 20 at%Ce in contrast to its absence in non-magnetic amorphous La_xSi_{100-x} alloys. As evidenced from Figs. 4(a), (b) and (c), a sharp upturn of the resistivity can be fitted to the logarithmic temperature dependence. Note that the data in (b) in the composition range $40 \leq x \leq 71$ deviate from the logarithmic dependence below the temperature marked by an arrow. As will be described below, this occurs in harmony with the spin-glass transition. The logarithmic temperature dependence was observed for all the alloys in the range $x \geq 15$ at%Ce. From this we conclude that the conduction electrons *do* exist and interact with randomly distributed magnetic moments associated with the localized Ce-4f electrons to give rise to the phenomenon reminiscent of the well-known incoherent Kondo effect in crystalline metals. Hence, amorphous alloys in this concentration range are identified as being in metallic regime.

The interaction between thermally excited electrons and

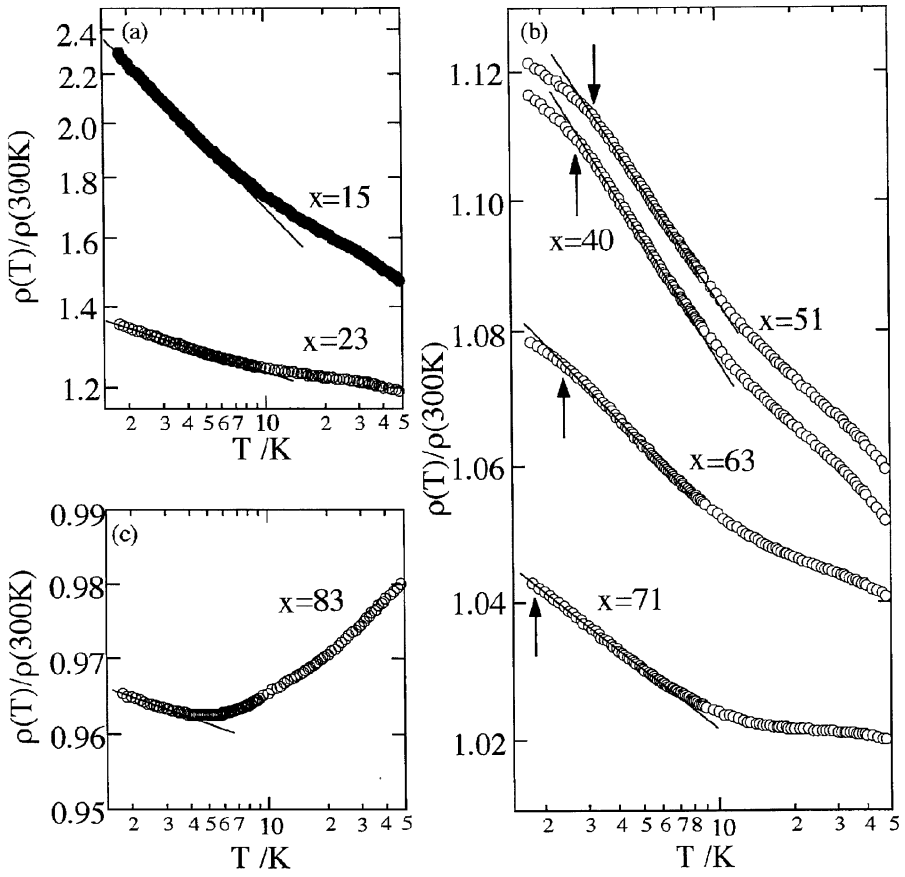

Fig. 4 Logarithmic temperature dependence of the normalized resistivity for amorphous Ce_xSi_{100-x} alloys with different compositions. Arrows in (b) indicate the spin-glass transition temperature (see Fig. 10).

magnetic moments should also take place in the insulating Ce_xSi_{100-x} alloy with $x \leq 12$. However, its behavior is different from that in the metallic regime. As shown in Fig. 3(b), the resistivity apparently rises with decreasing temperature without any indication of a sudden change in slope. In order to examine the conduction mechanism in insulating materials, it is customary to fit the temperature dependence of the measured conductivity to the following equation:

$$\sigma(T) = \sigma_0 \exp\left\{-\left(\frac{T_0}{T}\right)^n\right\}, \tag{1}$$

where $n = 1$, 1/2 and 1/4 are expected to hold for a system having a finite energy gap, the system characterized by the so called Coulomb gap due to the enhanced electron-electron interaction and the system obeying the variable-range hopping model proposed by Mott.[3)]

Since eq. (1) is rewritten as

$$\frac{d\ln\sigma(T)}{d\ln T} = n\ln\sigma_0 - n\ln\sigma(T), \tag{2}$$

we can experimentally determine the exponent n by plotting $\frac{d\ln\sigma(T)}{d\ln T}$ as a function of $\ln\sigma(T)$ for the present samples. As shown in Fig. 5, the exponent n turns out to be almost 1/4 for $x = 4$ and 5, to be closer to 1/2 for $x = 8$ and to unity for $x = 9$ and 12. For comparison, the exponent n is found to be close to 1/2 for the amorphous $La_{11}Si_{89}$ alloy. The possession of $n = 1$ or a hard energy gap for the amorphous $Ce_{12}Si_{88}$ alloy, which is located in the immediate vicinity of the insulating side of the metal-insulator transition, is a bit surprising, since the exponent $n = 1/2$ is deduced for the non-magnetic amorphous $La_{11}Si_{89}$ alloy. Indeed, as will be discussed in Section 3.5, the electronic specific heat coeffi-

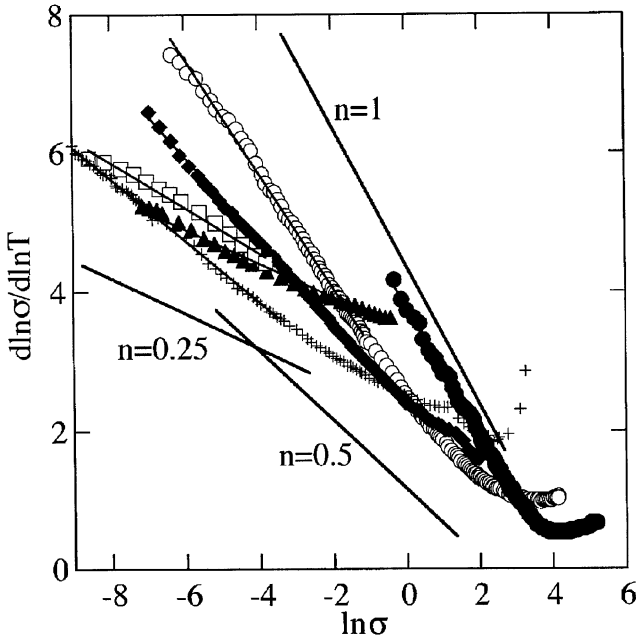

Fig. 5 $d\ln\sigma/d\ln T$ against $\ln\sigma$ for amorphous Ce_xSi_{100-x} alloys with different compositions: (□) $x = 4$, (▲) $x = 5$, (◆) $x = 8$, (○) $x = 9$, (●) $x = 12$ and (+) amorphous $La_{11}Si_{89}$ alloy. The slopes of $n = 1$, 0.5 and 0.25 are drawn as a guide to eye.

cient, which is derived from the specific heat data above 10 K, is still finite for the amorphous $Ce_{12}Si_{88}$ alloy. We believe that this seemingly inconsistent behavior stems from the fact that the gap opens up below about 10 K where the interaction between the thermally excited electrons and the localized magnetic moment becomes dominant, as will be discussed in the next Section. Here the energy gap of about 9 K is deduced by fitting the conductivity data below 8 K to eq. (1) with $n = 1$.

We must admit here that the lowest temperatures for the data with $x = 4$, 5, and 8 are limited above 10 K because of the difficulty in measuring too high resistivities. This made it difficult for us to extract the effect of localized moments on the electron transport properties, since such effect becomes appreciable only below 10 K in amorphous Ce–Si alloys as has been discussed above.

3.3 Electron transport measurements in magnetic fields

We found in the previous Section that the logarithmic temperature dependence of the resistivity is partly suppressed by the formation of the spin-glass state. Therefore, it is naturally expected that the external magnetic field will also affect the electron transport properties. As was discussed in Section 3.2, the amorphous $Ce_{15}Si_{85}$ alloy must be marginally metallic. We studied first the effect of magnetic field on the temperature dependence of the resistivity for this sample. The result is shown in Fig. 6(a). We revealed that the conductivity data below about 10 K are fitted to the logarithmic temperature dependence in the absence of magnetic field but are better fitted to the $\sqrt{T}$-dependence when measured in magnetic field of 9 T. The $\sqrt{T}$-dependence of conductivity below about 10 K is most likely attributed to the enhanced electron-electron interaction coupled with the weak localization in the metallic regime.[3] However, it may be noted here that the coefficient of the $\sqrt{T}$-term thus obtained is extremely large ($\sim 70\,\Omega^{-1}\mathrm{cm}^{-1}\mathrm{K}^{-1/2}$) in comparison with that observed in nonmagnetic amorphous alloys. The reason is not clear at the moment.

The suppression of the logarithmic temperature dependence of resistivity was similarly observed for all amorphous Ce_xSi_{100-x} ($15 \leq x \leq 83$) alloys under the magnetic field of 9 T. This validates our conjecture that the logarithmic temperature dependence of the resistivity *do* originate from spin fluctuations characteristic of the incoherent Kondo effect. As shown in Fig. 6(b), however, no measurable change in the temperature dependence of the electrical resistivity was observed in the non-magnetic amorphous $La_{19}Si_{81}$ alloy under the magnetic field of 9 T.

We also studied the effect of magnetic field on the temperature dependence of conductivity for amorphous Ce_xSi_{100-x} ($4 \leq x \leq 12$) insulators. As mentioned in Section 3.2, the exponent n was found to be close to unity for the $x = 9$ and 12 samples. Figure 7 shows $\frac{d\ln\sigma(T)}{d\ln T}$ plotted as a function of $\ln\sigma(T)$ for these samples under different magnetic fields. It is clear that the exponent n gradually decreases from unity and approaches 1/2 when the magnetic field is increased to 9 T. This may be interpreted in the following way. The presence of a finite value of γ in these insulators assures that electrons at the Fermi level are localized at absolute zero and that the hopping conduction due to thermally excited electrons dominates at finite temperatures. A hard energy gap with $n = 1$ would

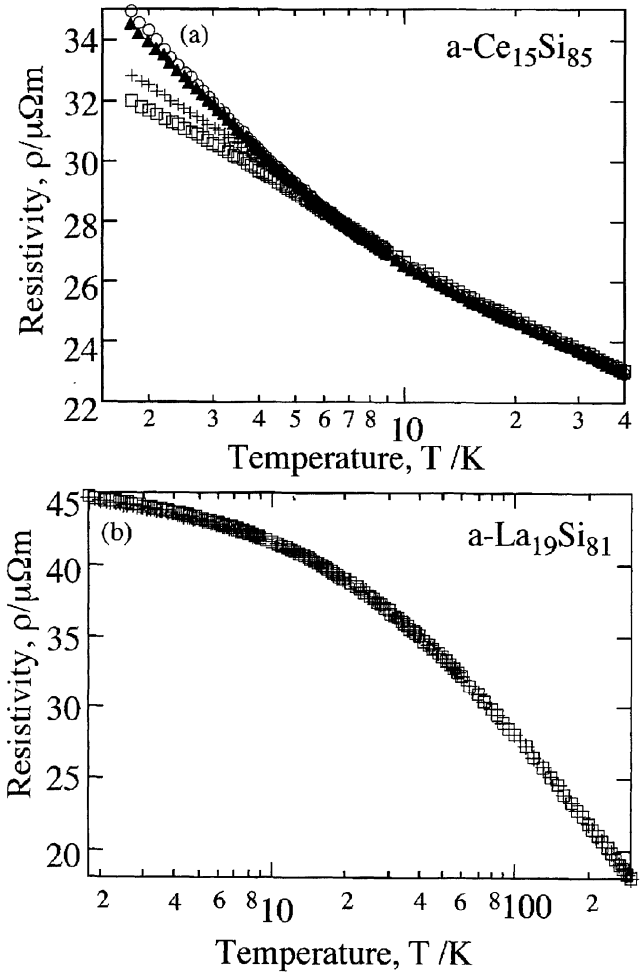

Fig. 6 Temperature dependence of electrical resistivity for (a) amorphous $Ce_{15}Si_{85}$ and (b) $La_{19}Si_{81}$ alloys under different magnetic fields: (○) 0 T, (▲) 1 T, (+) 5 T and (□) 9 T.

be formed as a result of the formation of a bound state through the screening of Ce-4f localized moments by these thermally excited hopping electrons in the manner similar to the Kondo effect in metallic regime.[12] However, an increase in magnetic field certainly contributes to suppressing spin fluctuations of Ce-4f localized moments and, hence, the exponent n tends to decrease to 1/2 due to gradually diminishing energy gap.

3.4 Magnetic measurements

As is clear from the discussion above, the Kondo effect is found to dominate at low temperatures so that we need to know how the magnetic state changes as a function of the Ce concentration in order to deepen the understanding of the electron transport mechanism across the metal-insulator transition in this system. Figure 8 depicts the temperature dependence of $(\chi - \chi_0)^{-1}$ measured in the applied field of 39.8 kA/m for amorphous Ce_xSi_{100-x} ($x = 4$, 15, 51, 63 and 83) alloys, where χ is the measured magnetic susceptibility and χ_0 is the temperature independent term described below. The data in the temperature range 100–300 K are well approximated by a straight line and, thus, fitted to the following equation known as the Curie-Weiss law:

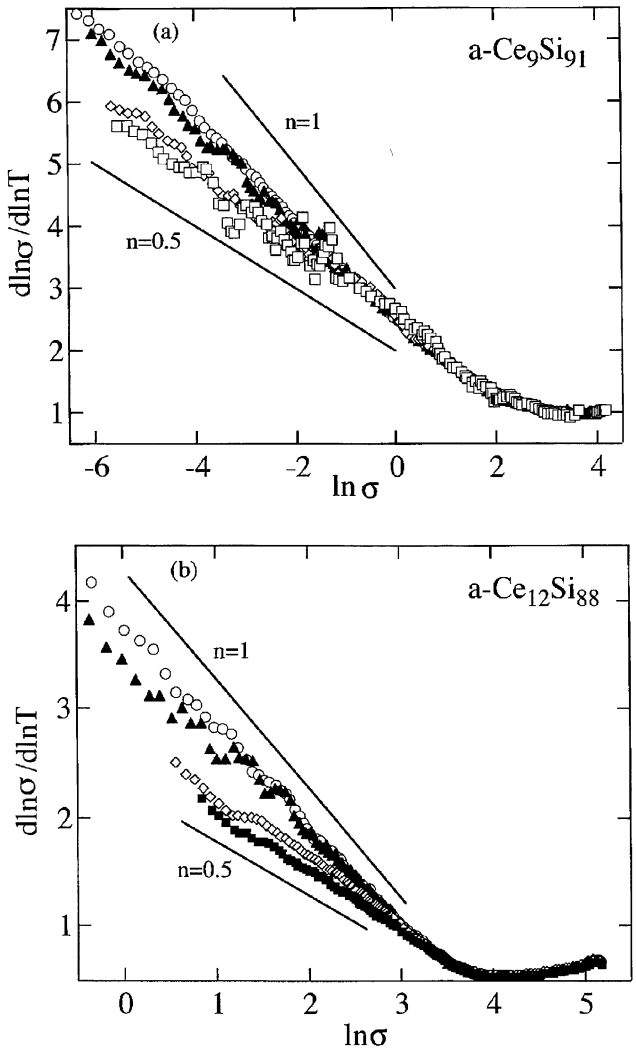

Fig. 7 $d\ln\sigma/d\ln T$ against $\ln\sigma$ for amorphous (a) Ce_9Si_{91} and (b) $Ce_{12}Si_{88}$ alloys measured under different magnetic fields: (○) 0 T, (▲) 1 T, (◇) 5 T and (◆) 9 T. The slopes of $n = 1$ and 0.5 are drawn as a guide to eye.

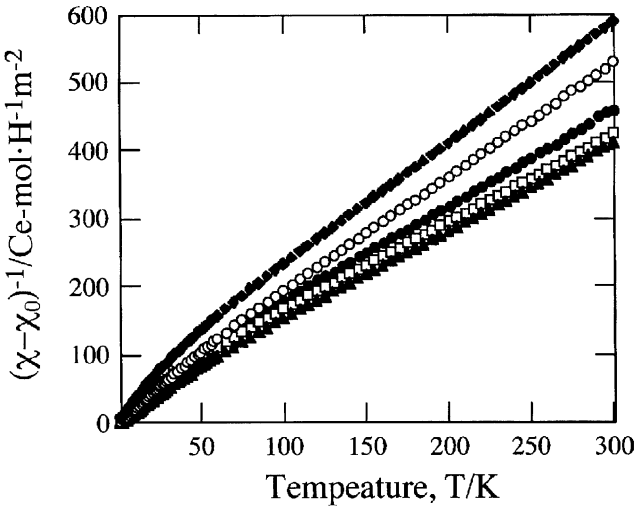

Fig. 8 Temperature dependence of the inverse of magnetic susceptibility measured in the applied field of 500 Oe for amorphous Ce_xSi_{100-x} alloys with different compositions: (●) $x = 4$, (□) $x = 15$, (▲) $x = 51$, (○) $x = 63$ and (◆) $x = 83$.

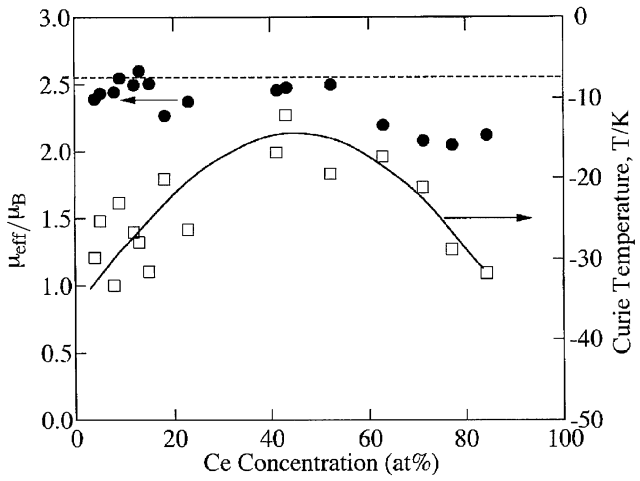

Fig. 9 Ce concentration dependence of (●) effective magnetic moment $\mu_{\rm eff}$ and (□) Curie temperature for a series of amorphous Ce_xSi_{100-x} alloys.

$$\chi = \chi_o + \frac{C}{T - \theta_p}, \tag{3}$$

where χ_o is the temperature independent Pauli paramagnetic susceptibility, C is the Curie constant and θ_p is the paramagnetic Curie temperature. The effective magnetic moment $\mu_{\rm eff}$ is calculated from the Curie constant C by using the relation:

$$\mu_{\rm eff} = \sqrt{\frac{3k_B C}{N}}\mu_B, \tag{4}$$

where N is the number of Ce atoms carrying the localized moment, k_B is the Boltzmann constant and μ_B is the Bohr magneton.

The resulting paramagnetic Curie temperature θ_p and effective magnetic moment $\mu_{\rm eff}$ are plotted in Fig. 9 as a function of the Ce concentration x. The value of θ_p is negative for all samples, indicating the existence of antiferromagnetic coupling between the localized moments. Its absolute value exhibits a minimum in the vicinity of $x = 50$. On the other hand, the effective magnetic moment is rather close to the value of 2.54 for the Ce^{3+} free ion. However, there is a definite tendency for the effective moment to decrease with increasing Ce concentration. This might be deeply related to the manifestation of the enhanced electronic specific heat coefficient observed above 10 K, as will be discussed in the next Section. It is also noted that the antiferromagnetic interaction between the localized moments becomes weak in the vicinity of $x = 50$.

The temperature dependence of the magnetic susceptibility for samples in the range $40 \leq x \leq 71$ was more carefully studied by using further lower applied magnetic field of 0.8 kA/m. As shown in Fig. 10, we observed the different temperature dependences below the so called spin freezing temperature T_f, depending on the field cooling (FC) or zero-field cooling (ZFC) modes. This means that the spin-glass state is stabilized below T_f. As mentioned earlier in connection with Fig. 4(b), a change in slope is also observed at T_f in the temperature dependence of the electrical resistivity. Therefore, we found that the RKKY interaction dominates at temperatures below T_f in the intermediate concentration range

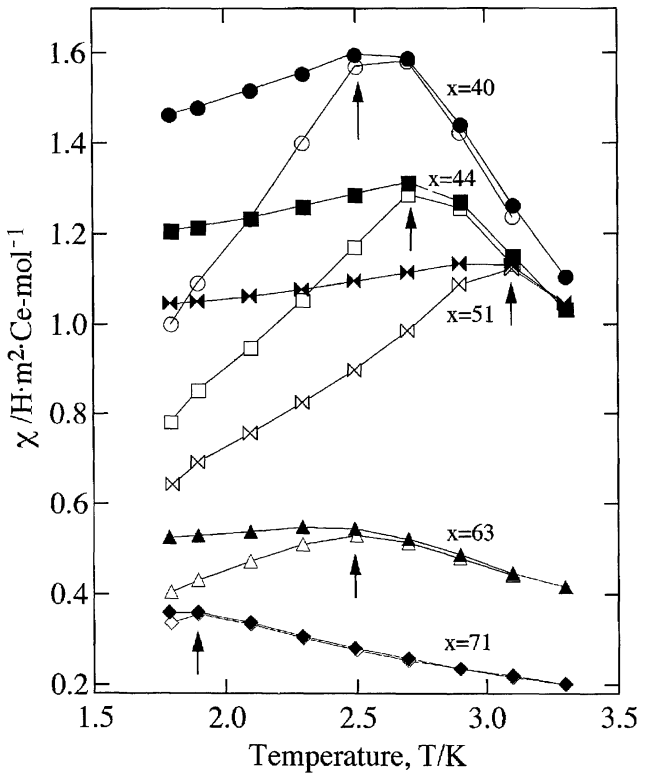

Fig. 10 Temperature dependence of magnetic susceptibility for amorphous Ce_xSi_{100-x} alloys (x = 40, 44, 51, 63 and 71) measured in the applied field of 0.8 kA/m in both FC and ZFC modes. The spin freezing temperature T_f is marked by arrows.

$40 < x < 70$.

Figure 11 shows the Ce concentration dependence of the spin freezing temperature along with magnetization at 2 K measured under the applied field of 7 T. The spin-glass state is found in the concentration range centered at $x = 50$. It is interesting to note that the magnetization at 2 K shows a unique Ce concentration dependence: its value is rather large in the insulating regime, where only thermally excited carriers are present, and also in the range where the spin-glass state appears at low temperatures. We may alternatively say that the magnetization at 2 K is apparently reduced in the concentration range, where the incoherent Kondo effect dominates down to the lowest temperatures. We consider this behavior to be consistent because the localized moment tends to be screened by conduction electrons.

3.5 Low temperature specific heat measurement

The specific heat C was measured for amorphous Ce_xSi_{100-x} (x = 4, 9, 15, 51 and 63) alloys over the temperature range 0.5–20 K. As representative we show in Fig. 12 the temperature dependence of specific heat for the amorphous $Ce_{15}Si_{85}$ alloy. Since the specific heat for the nonmagnetic metal is well represented by $\gamma T + \alpha T^3$, a broad peak observed at about 2 K is most likely attributable to the anomalous specific heat due to the Ce-4f localized electrons. Here, γ and α represent electronic and lattice specific heat coefficients, respectively. The inset in Fig. 12 shows the same data in the form of C/T versus T^2. A straight line fitting is possible for high temperature data, as shown in the inset. The electronic specific heat coefficient and the Debye temperature for the $x = 15$ sample are deduced from its intercept and slope to be 22.5 mJ/mol·K^2 and 314 K, respectively. The electronic specific heat thus obtained is about 50 times as large as the value of 0.4 mJ/mol·K^2 for the marginally metallic amorphous $Ti_{13}Si_{87}$ alloy. This implies that the contribution of 4f-electrons to the electronic specific heat is apparently already significant even above 10 K in amorphous Ce–Si alloys in metallic regime, as well as below 10 K, where the Schottky-like specific heat anomaly is superimposed. The electronic specific heat coefficient for other samples is determined in the same manner as described above. Numerical data are listed in Table 1.

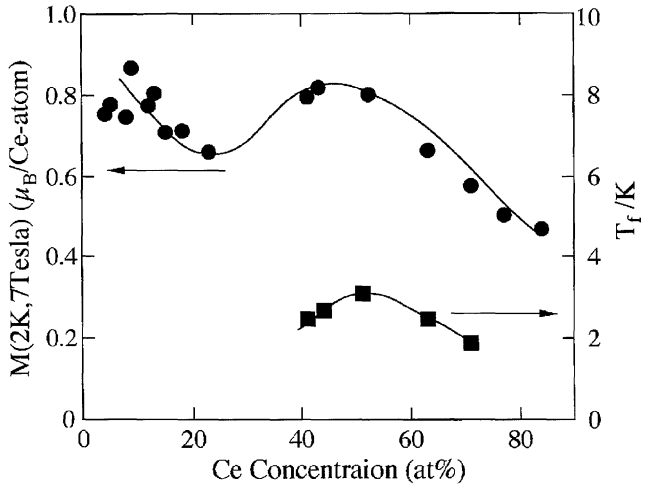

Fig. 11 Ce concentration dependence of the spin freezing temperature T_f and magnetization at 2 K measured under the applied field of 7 T for amorphous Ce_xSi_{100-x} alloys.

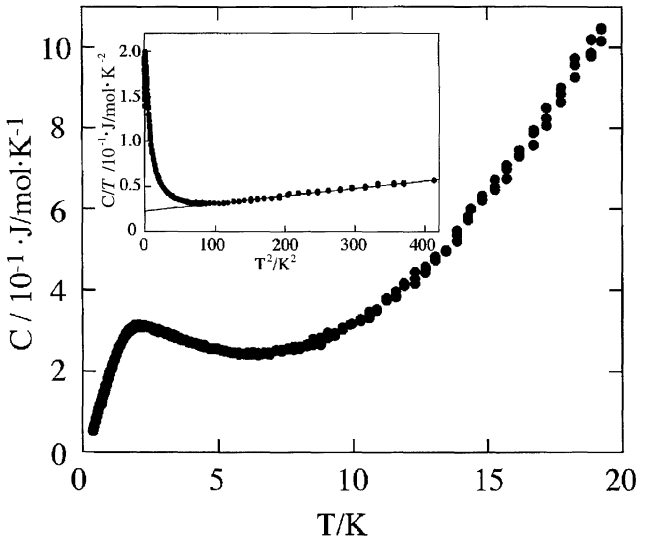

Fig. 12 Temperature dependence of specific heat C for the amorphous $Ce_{15}Si_{85}$ alloy. Inset shows the same data in the form of C/T versus T^2.

In order to gain more insight into the anomalous specific heat, we measured the specific heat for the two samples with $x = 15$ and 51 in the presence of magnetic fields of 1 and 5 T. Figure 13 shows the anomalous specific heat ΔC for the $x = 15$ sample after subtracting the normal specific heat given by the sum of the electronic and lattice specific heats estimated above. The peak position is found to shift to higher temperatures with increasing magnetic field. We believe the

anomalous specific heat to be the phenomenon associated with the 4f-levels of Ce^{3+} ion, which is responsible for the occurrence of the logarithmic temperature dependence of resistivity. The Ce^{3+} ion is known to possess Kramer's two-fold degenerate state as a ground state. We assume that the degenerate state is lifted in the crystalline field of the amorphous matrix and that only the two-level state is responsible for the observed anomalous specific heat below 10 K. The energy interval δ between the two levels expands with increasing magnetic field due to the Zeeman splitting and is expressed as

$$\delta(H) = \delta_0 + \frac{\mu_B g J_z H}{k_B}, \tag{5}$$

where g is the Landé g-factor, J_z is the z-component of the total angular momentum and δ_0 is the energy interval of the two levels in the absence of magnetic field. The temperature T_{max} corresponding to the peak of the anomalous specific heat is given by

$$T_{max} = 0.42\delta \tag{6}$$

in the two-level Schottky model.[13] By inserting measured T_{max} values and $g = 6/7$ for the Ce^{3+} ion into eqs. (5) and (6), we can easily deduce $J_z = 2.28$ for the Ce^{3+} ion. The J_z value thus obtained is fairly close to $J = 5/2 = 2.5$ for the Ce^{3+} free ion, indicating that the present analysis is basically correct despite that the two-level model may be too simple.

The excess entropy due to the Schottky specific heat is calculated as

$$\Delta S(T) = \int_0^T \frac{\Delta C}{T} dT, \tag{7}$$

where ΔC is the anomalous specific heat discussed above. The temperature dependence of the excess entropy is shown in Fig. 14 for the two samples with $x = 15$ and 51. Since there exist the two-level states in this temperature range, the excess entropy should approach the value of $R \ln 2$, where R is the gas constant. The saturated value of ΔS is only 56 and 47% of the theoretical value of $R \ln 2$. This implies that almost half of Ce atoms bear the localized moment of 2.5 μ_B and that the Ce-4f electrons donated by remaining half Ce atoms contribute to the γT term responsible for the enhanced electronic specific heat coefficient discussed above.

It is worthwhile mentioning at this stage that the specific heat data demonstrating only one half of Ce atoms to bear the localized magnetic moments, are seemingly inconsistent with the magnetic data discussed in Section 3.4, where all Ce^{3+} ions are claimed to possess the magnetic moment of 2.54 μ_B. Note here that the specific heat data represent the Ce-4f states below 20 K whereas the Curie-Weiss fitting is applicable only in the temperature range 100–300 K. In summary, all the experimental data so far presented lead us to conclude that the interaction of the magnetic moment due to Ce^{3+} ion with conduction electrons is less important above 100 K but becomes crucially important below about 20 K.

3.6 Photoemission spectroscopy measurement

We have also studied the valence band structure by means of the X-ray photoemission spectroscopy (XPS) measurements for amorphous Ce_xSi_{100-x} (x = 9, 18, 52, 63, 85 and 100) alloys including pure Ce. The XPS spectra were measured over binding energies up to 28 eV and background contributions were properly subtracted. As shown in Fig. 15(a), the peak area due to localized Ce-4d states centered at about 18 eV is reasonably assumed to be proportional to the Ce concentration. Now the valence band spectra are normalized with respect to the Ce concentration by using the peak area of Ce-4d states and are shown in Fig. 15(b) over binding energies up to 5 eV. The density of states at the Fermi level is clearly found to decrease with decreasing Ce concentration. The Fermi cut-off is clearly seen in amorphous $Ce_{18}Si_{82}$ sample but is apparently absent in the insulating Ce_9Si_{91} sample.

The high-resolution ultra-violet photoemission spectrum was measured at 8 K by using the HeI excitation energy

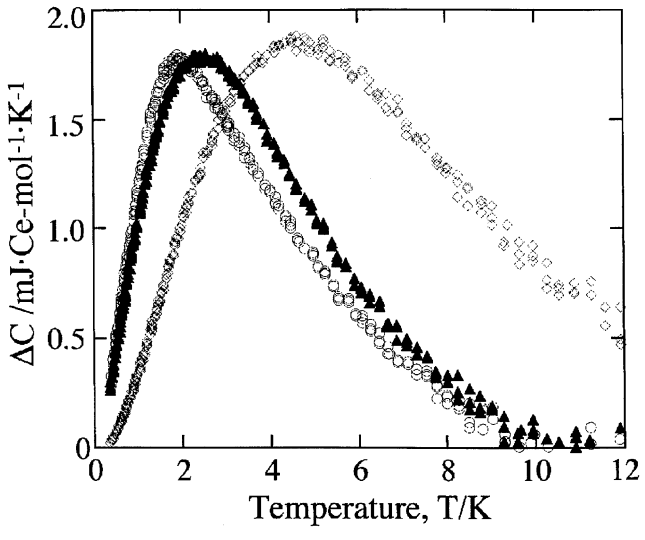

Fig. 13 Temperature dependence of anomalous specific heat ΔC for the amorphous $Ce_{15}Si_{85}$ alloy under different magnetic fields: (○) 0 T, (▲) 1 T and (◇) 5 T. Note that the specific heat is now in the units of mJ/Ce-mol·K.

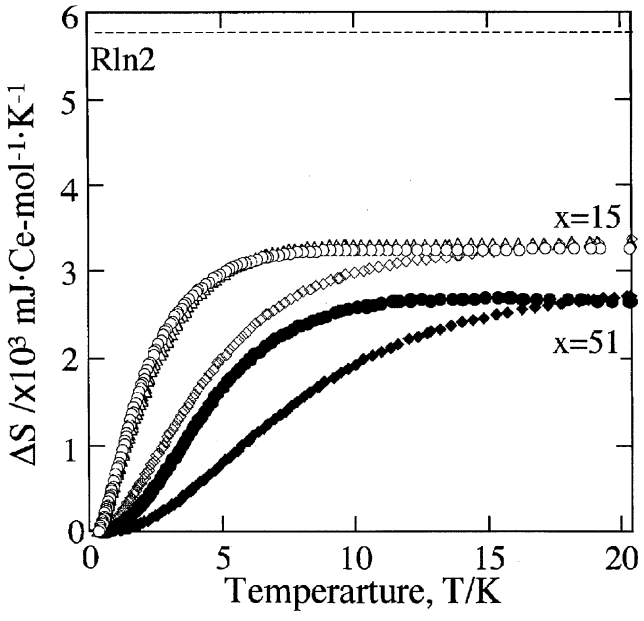

Fig. 14 Temperature dependence of the excess entropy associated with the two-level Schottky anomaly for the amorphous $Ce_{15}Si_{85}$ and $Ce_{51}Si_{49}$ alloys. (○, ●) 0 T, (△) 1 T and (◇, ◆) 5 T. The line of $R \ln 2$ represents the theoretical limit of the excess entropy in the two-level system.

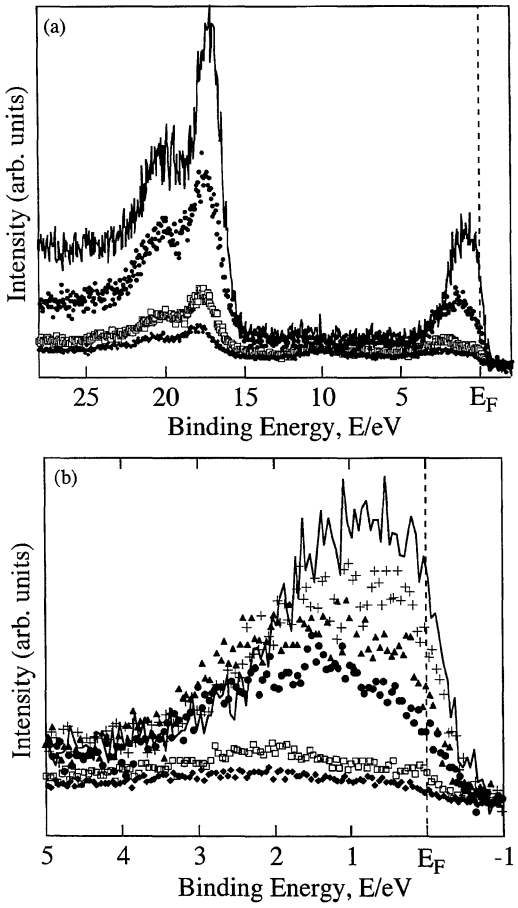

Fig. 15 XPS spectra in binding energies up to (a) 28 and (b) 5 eV for amorphous Ce_xSi_{100-x} alloys with different compositions: (◆) $x = 9$, (□) $x = 18$, (●) $x = 52$, (▲) $x = 63$, (+) $x = 85$ and (—) pure Ce.

($h\nu = 21.218$ eV) for the amorphous $Ce_{15}Si_{85}$ sample together with pure Au as a reference. The spectrum is shown in Fig. 16. One can clearly see a sharp Fermi-cutoff, being well consistent with our conclusion that this alloy is indeed in metallic regime. However, sharp peaks or their tail associated with 4f-electrons[14] are not visible, at least, within the measured energy range of 160 meV from the Fermi level. In order to ascertain if the localized 4f-states remain immediately below the Fermi level or not, we consider it necessary to perform the photoemission measurement over binding energies down to 1 eV by using the He II radiation, since the ratio of the 4f- over spd-electron cross sections increases by a factor of 10 when the excitation energy increases from 21 to 42 eV.

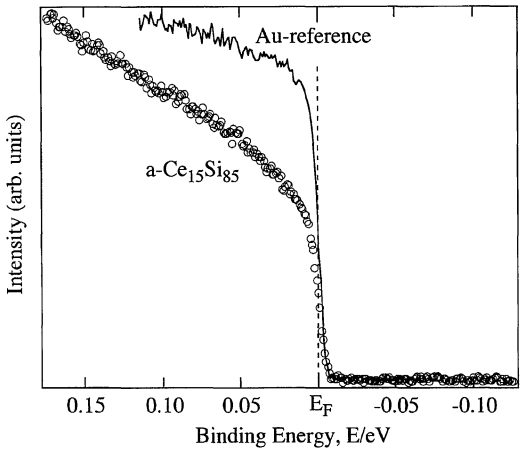

Fig. 16 UPS valence band spectrum for the amorphous $Ce_{15}Si_{85}$ alloy in binding energies within 0.1 eV from the Fermi level measured at 8 K. Note the presence of a sharp Fermi cut-off and smallness of thermal energies of only 0.002 eV.

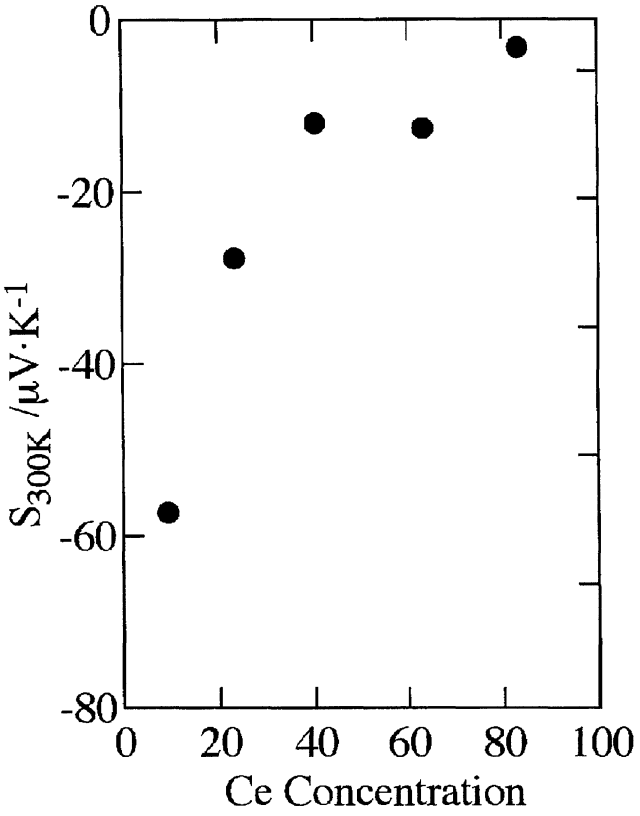

Fig. 17 Ce concentration dependence of the Seebeck coefficient at 300 K for amorphous Ce_xSi_{100-x} alloys.

3.7 Thermoelectric properties

The Seebeck coefficient was measured over the temperature range 100–400 K for amorphous Ce_xSi_{100-x} ($x = 9$, 23, 40, 63 and 83) alloys. The temperature dependence is roughly linear in temperature in metallic regime. As shown in Fig. 17, the Seebeck coefficient at 300 K increases in a negative direction with approaching the metal-insulator transition from a metallic side and the largest value of $-55\,\mu$V/K is achieved for the $x = 9$ insulator. Unfortunately, we could not obtain the Seebeck coefficient exceeding $\pm 100\,\mu$V/K like in many thermoelectric materials even in the composition range, where the Fermi level falls in the pseudogap, *i.e.*, in the metallic side near the metal-insulator transition. The Seebeck coefficient is known to be enhanced near the Kondo temperature in heavy fermion systems due to the interaction between the conduction electrons and localized moments.[15] Unfortunately, we could not observe any anomalous enhancement due presumably to the limited measuring temperature range down to 100 K. We expect an enhancement in the Seebeck coefficient in the present Ce–Si alloys to occur at further lower temperatures, say, below 20 K, where the interaction of the conduction electrons and localized moment becomes strong.

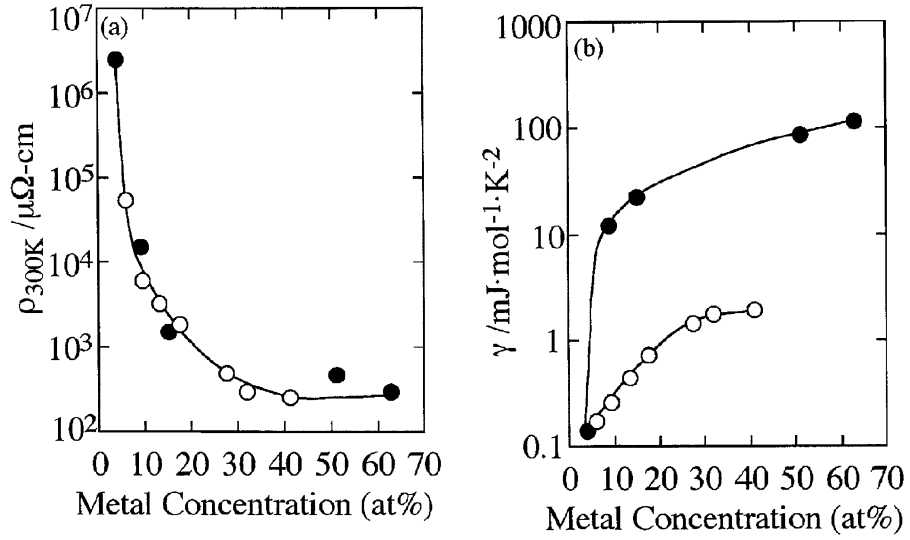

Fig. 18 Metal concentration dependence of (a) electrical resistivity at 300 K and (b) electronic specific heat coefficient for amorphous (●) Ce_xSi_{100-x} and (○) Ti_xSi_{100-x} alloys.

4. Discussion

Mizutani discussed universal features associated with the metal-insulator transition in many different systems including crystalline compounds, quasicrystals, amorphous alloys and strongly correlated electron systems by plotting the measured resistivity ρ at 300 K against the measured electronic specific heat coefficient γ on the log-log scale.[3] The resistivity or conductivity σ in the metallic regime was then analyzed in terms of the Mott conductivity formula given by

$$\sigma = \rho^{-1} = g^2 S_F^{free} e^2 a / 12\pi^3 \hbar, \tag{8}$$

where g is the ratio of the DOS at E_F over the corresponding free electron value, S_F^{free} is the area of the free electron Fermi sphere, a is an average atomic distance.[3] Note that eq. (8) is derived without taking into account the quantum interference effect. Therefore, it should be applied to the pseudogap system with the g-parameter varying over $0 < g < 1$ at temperatures high enough for the weak localization effect to be ignored. This is the reason why the resistivity at 300 K was chosen rather than residual resistivity in the ρ-γ diagram. As mentioned in Introduction, a line $\rho = (\pi^2/3)(k_B/e)^2 D_{min}^{-1} \gamma^{-1}$ with a slope of -1 can be drawn in the ρ-γ diagram, where D_{min} is set equal to $0.25\,cm^2/s$. This is called the metal-insulator transition line (MI-line), above which insulators should appear in principle regardless of the magnitude of the density of states at E_F.

Figure 18 shows the solute concentration dependence of the resistivity at 300 K and the electronic specific heat coefficient for amorphous Ce_xSi_{100-x} alloys in comparison with those for the amorphous Ti_xSi_{100-x} alloys.[7] There is no substantial difference in the resistivity behavior but, instead, a large discrepancy appears in the behavior of the electronic specific heat coefficient. It is, therefore, of great interest to examine how the amorphous Ce_xSi_{100-x} alloys behave in the ρ-γ diagram.

Figure 19 summarizes the ρ_{300K}-γ_{exp} diagram on log-log scale, in which the data for different pseudogap systems are plotted, including those of quasicrystals,[3] amorphous V_xSi_{100-x}[6] and Ti_xSi_{100-x}[7] alloys together with the present amorphous Ce_xSi_{100-x} alloys. We emphasized in Section 3.5 that the number of Ce ions bearing the localized magnetic moment of 2.54 μ_B is strongly temperature dependent, indicating that the Ce-4f states at 300 K differ from those at low temperatures below about 20 K. Therefore, it may not be legitimate to plot ρ_{300K} against the value of γ determined at low temperatures in the case of the amorphous Ce–Si alloys. Fortunately, however, the ratio of ρ_{4K} over ρ_{300K} in metallic regime is at most two even for the marginally metallic sample with $x = 15$ so that whether we choose ρ_{4K} or ρ_{300K} is of minor importance on log-log scale for samples in metallic regime.

First, we briefly discuss the data for quasicrystals and amorphous V_xSi_{100-x} and Ti_xSi_{100-x} systems in the metallic regime prior to the discussion of the present system. In the case of quasicrystals, the resistivity is found to increase with decreasing the DOS at E_F and to cross the MI-line in the limit of vanishing DOS at E_F. Moreover, the data fall on a universal line with the slope of -2 in agreement with the Mott conductivity formula given by eq. (8). The data for amorphous V_xSi_{100-x} alloys with $x > 20$ also fall on a straight line with a slope of -2 in excellent agreement with the Mott conductivity formula. However, we realize that the line, which may be called the Mott-line, is substantially shifted to the right relative to the Mott-line for quasicrystals discussed above. In addition, it should be noted in Fig. 19 that the data points with $x \leq 14$ marked with symbol (▼), which represent the data in the insulating regime, deviate substantially from the Mott-line drawn through the metallic samples. In contrast to the case in quasicrystals, the amorphous V-Si pseudogap system enters into an insulating regime by crossing the MI-line at a finite γ_{exp} value on the ρ-γ_{exp} diagram.

The data for amorphous Ti_xSi_{100-x} alloy system in the metallic regime also fall on the Mott-line with a slope of -2 but deviate from it when it enters into the insulating regime. It is noted that the Mott-line apparently shifts more to the right with increasing the number of d-electrons of the transition metal element involved. In other words, the Fermi velocity v_F

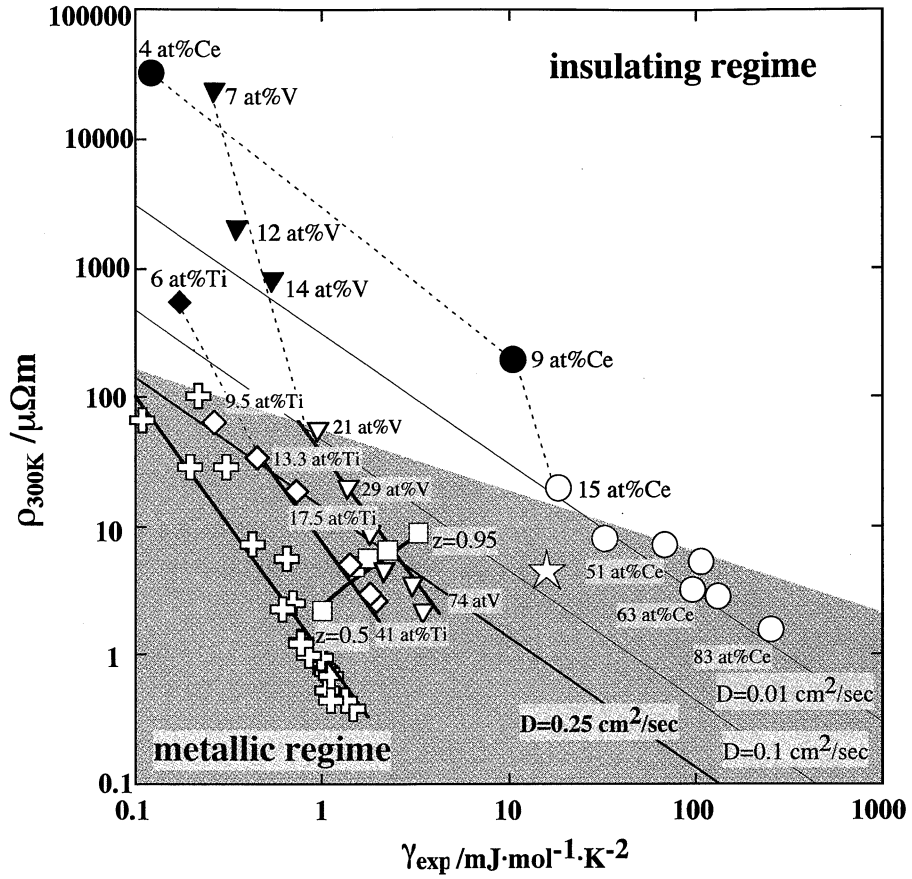

Fig. 19 Resistivity at 300 K against γ_{exp} value on the log-log scale for (○, ●) amorphous Ce_xSi_{100-x} alloys, (✠) quasicrystals and approximants[3]), (▽, ▼) amorphous V_xSi_{100-x} alloys,[6] (◇, ◆) amorphous Ti_xSi_{100-x} alloys,[7] (□) $Sr_{1-z}La_zTiO_3$[16] and (☆) Fe_2VAl[17]). Open and filled symbols refer to samples characterized as metallic and insulating states, respectively. The data for amorphous M_xSi_{100-x} (M = Ti and V) alloys in the metallic regime as well as quasicrystals are fitted to lines with the slope of -2 consistent with the Mott conductivity formula.[3] The shaded area represents the experimentally determined metallic regime.

in the amorphous M-X alloy system with the transition metal element M situated to the right in the periodic table is lower than that in the system with M situated to the left, when a comparison is made at a given $N(E_F)$ or the electronic specific heat coefficient. *This may be taken as an indication that 3d-electrons at E_F are partially localized even in the metallic regime and that their number apparently increases with increasing the number of d-electrons of the element M in the amorphous M_xSi_{100-x} alloys.*

As discussed above, amorphous Ce_xSi_{100-x} alloys are characterized as a system where the electronic specific heat coefficient is greatly enhanced but the electrical resistivity is comparable to that found in amorphous Ti_xSi_{100-x}[7] alloys (see Fig. 18). With decreasing Ce concentration, the electronic specific heat coefficient *does* decrease down to about 22 mJ/mol·K^2 before the transition to the insulating regime at the Ce concentration of about 12 at%. The data for amorphous Ce_xSi_{100-x} alloys are incorporated in Fig. 19, together with the data from literature.[11] It is clear that the ρ-γ data are located far to the right in the diagram and that the data in metallic regime fall on a line with a slope of almost -1 instead of -2 arising from the Mott conductivity formula. It is also seen that the data deviate substantially from the line fitted to metallic ones when entering into the insulating regime.

In the case of amorphous V-Si and Ti-Si alloys, the number of electrons at the Fermi level, being mostly composed of V-3d and Ti-3d electrons, remain finite even in the insulating regime and these localized electrons give rise to the variable-range hopping conduction. However, most of these electrons become mobile and manifest the weak localization effect in the metallic regime. In the case of amorphous Ce–Si alloys, the situation is apparently different. Electrons at the Fermi level are composed of Si-3p, Ce-5d and Ce-6s electrons in addition to Ce-4f electrons. We may consistently interpret the unusual location of the ρ-γ data in amorphous Ce–Si alloys, only if we can assume that the Ce-4f electrons contributing to the specific heat γT are still immobile even in the metallic regime. This means that the Fermi velocity of these 4f-electrons should be much smaller and, in turn, the effective mass is much heavier than that of other electrons at the Fermi level, thereby 4f-electrons at the Fermi level being essentially localized and participating in the electron conduction only via the variable-range hopping mechanism. Of course, the variable-range hopping conduction in metallic regime with $x \geq 15$ is completely masked by the presence of other mobile electrons at the Fermi level.

All data points marked by open symbols in Fig. 19 have to be regarded as a metal. The region encompassing open symbols is shown as a shaded area. Thus, the boundary represents an experimentally determined metal-insulator boundary. We see that the metallic regime apparently extends well above the MI-line of $D_{min} = 0.25\,cm^2/s$, when the value of γ_{exp} be-

comes large.

Finally, a brief comment is made on other unique metallic systems, in which the datasets ($\rho_{300\,\mathrm{K}}$, γ_{exp}) definitely fail to obey the Mott conductivity formula. The data for $Sr_{1-z}La_zTiO_3$,[16] being typical of a strongly correlated electron system, are included in Fig. 19 for the composition range $0.5 \leq z \leq 0.95$ (see open square). The $z = 0.95$ sample is still in the metallic regime while the $LaTiO_3$ with $z = 1.0$ is an insulator. The marginally metallic $z = 0.95$ sample falls slightly above the MI-line of $D_{\mathrm{min}} = 0.25\,\mathrm{cm^2/s}$ in the $\rho_{300\,\mathrm{K}} - \gamma_{\mathrm{exp}}$ diagram. However, the data points in the metallic regime obviously no longer follow the Mott conductivity formula (8).

Nishino *et al.*[17,18] found that the $D0_3$-type Fe_2VAl intermetallic compound exhibits the semiconductor-like temperature dependence of the electrical resistivity and that its resistivity of 850 μΩ-cm at 300 K increases to 3000 μΩ-cm at 4.2 K, though the photoemission spectroscopy measurement revealed a sharp Fermi cut-off. This system is also classified as a pseudogap system, since E_{F} is located in a deep pseudogap. Nevertheless, the electronic specific heat coefficient is deduced to be $14\,\mathrm{mJ/mol{\cdot}K^2}$ and its large enhancement is ascribed to the spin fluctuations unique to a marginally magnetic alloy. The set of ($\rho_{300\,\mathrm{K}}$, γ_{exp}) data for this compound falls in the region close to $D = 0.1\,\mathrm{cm^2/s}$ line in the ρ-γ_{exp} diagram again well above the classical MI-line of $D_{\mathrm{min}} = 0.25\,\mathrm{cm^2/s}$.

5. Conclusion

The electronic structure, magnetism and electron transport properties of the amorphous Ce_xSi_{100-x} alloys have been studied over a wide Ce concentration range $4 \leq x \leq 83$. Main conclusions are listed below.

(1) The metal-insulator transition is found to occur at about 12 at%Ce.

(2) The interaction between conduction electrons and localized moments due to Ce^{3+} ions is essentially neglected above 100 K but becomes substantial below about 20 K, leading to an anomalous enhancement in the temperature dependence of the resistivity below 10 K.

(3) The successful Curie-Weiss fitting of the magnetic susceptibility data led us to conclude that all the Ce atoms bear the localized magnetic moment of $2.54\,\mu_{\mathrm{B}}$ above about 100 K. However, the coexistence of the Schottky specific heat and T-linear specific heat confirmed that only half of Ce atoms remain to bear the localized magnetic moment while 4f-electrons donated by the remaining Ce atoms contribute to the electronic specific heat γT below about 20 K. This points to the fact that both electronic structure and magnetism associated with Ce-4f states are strongly temperature dependent.

(4) Though the value of $\rho_{300\,\mathrm{K}}$ is comparable to those in the reference systems La–Si and Ti–Si, the value of γ of the marginally metallic $Ce_{15}Si_{85}$ alloy is 50 times as large as that for the marginally metallic $Ti_{13}Si_{87}$ alloy. This provided us a unique opportunity to explore the conduction mechanism of electrons involving Ce-4f electrons at the Fermi level in the amorphous Ce_xSi_{100-x} alloys.

(5) The Ce-4f electrons contributing to the specific heat γT are found to be essentially localized even in the metallic regime for the Ce concentration range $x \geq 15$. The electron conduction in the metallic regime is dominated by electrons arising from the Si-3p, Ce-6s and Ce-5d states at the Fermi level. This explains well the reason why the data of the amorphous Ce_xSi_{100-x} alloys fall on a diffusion coefficient line of only $D = 0.01\,\mathrm{cm^2/s}$ in the $\rho_{300\,\mathrm{K}} - \gamma$ diagram.

6. Acknowledgments

We are grateful to Professor S. Shin, the University of Tokyo, for allowing us to measure the high-resolution UPS spectra for the amorphous Ce–Si alloy. We also express our thanks to Professor H. Ikuta and Dr. A. Rogatchev for fruitful discussion during the course of this study.

REFERENCES

1) N. F. Mott: Philos. Mag. **13** (1966) 989–1014.
2) U. Even and J. Jortner: Phys. Rev. Lett. **28** (1972) 31–34.
3) U. Mizutani: *Introduction to the Electron Theory of Metals*, (Cambridge University Press, 2001) Chapter 15, pp.
4) H. Sato, T. Takeuchi and U. Mizutani: Phys. Rev. B. (2001) submitted to Phys. Rev. B.
5) T. Takeuchi, T. Onogi, E. Banno and U. Mizutani: Mater. Trans. **42** (2001) 933–938.
6) U. Mizutani, T. Ishizuka and T. Fukunaga: J. Phys.: Condensed Matter **9** (1997) 5333–5353.
7) A. Rogatchev, T. Takeuchi and U. Mizutani: Phys. Rev. B **61** (2000) 10010–10014.
8) K.Tanaka, K. Furui and M. Yamada: J. Phys. Soc. Jpn. **64** (1995) 4790–4798.
9) A. C. Hewson: *The Kondo Problem to Heavy Fermions*, (Cambridge University Press, 1993).
10) T. Nishioka, Y. Uchida, S. Chikazawa and M. Kontani: Physica B **230–232** (1997) 189–191.
11) T. Hihara, K. Sumiyama, H. Yamauchi, Y. Homma, T. Suzuki and K. Suzuki: J. Phys.: Condensed Matter **5** (1993) 8425–8436.
12) P. Dai, Y. Zhang and M. P. Sarachik: Phys. Rev. Lett. **69** (1992) 1804–1806.
13) E. S. R. Gopal: *Specific Heat at Low Temperatures*, (Plenum Press, 1966) pp. 102–105.
14) F. Patthey, W. D. Schneider, Y. Baer and B. Delley: Phys. Rev. Letters **58** (1987) 2810–2813.
15) Y. Onuki and T. Komatsubara: J. Mag. Mag. Mater. **63&64** (1987) 281–288.
16) Y. Tokura, Y. Taguchi, Y. Okada, Y. Fujimori, T. Arima, K. Kumagai and Y. Iye: Phys. Rev. Letters **70** (1993) 2126–2129.
17) Y. Nishino, M. Kato, S. Asano, K. Soda, M. Hayasaki and U. Mizutani: Phys. Rev. Letters **79** (1997) 1909–1912.
18) Y. Nishino: Mater. Trans. **42** (2001) 902–910.